Information Sciences 586 (2022) 279–293

Contents lists available at ScienceDirect

Information Sciences

journal homepage: www.elsevier.com/locate/ins

Multiscale increment entropy: An approach for quantifying the physiological complexity of biomedical time series

Xue Wang [a,b], Xiaofeng Liu [a,c,d,*], Wei Pang [e], Aimin Jiang [a,c,d]

[a] College of IoT Engineering, Hohai University, Changzhou 213022, PR China
[b] School of Microelectronics and Control Engineering, Changzhou University, Changzhou 213164, PR China
[c] Jiangsu Key laboratory of Special Robot Technology, Changzhou 213022, PR China
[d] Changzhou Key Laboratory of Special Robot and Intelligent Technology, Changzhou 213022, PR China
[e] School of Mathematical and Computer Sciences, Heriot-Watt University, Edinburgh, Scotland EH14 4AS, UK

ARTICLE INFO

Article history:
Received 26 September 2020
Received in revised form 17 November 2021
Accepted 23 November 2021
Available online 1 December 2021

Keywords:
Increment entropy
Multiscale analysis
Physiological complexity
Physiological time series

ABSTRACT

Time series data recorded from physiological systems often innately exhibit inherent physiological complexity variation on a long-range temporal scale. Multiscale analysis is considered vital for characterising the features of physiological signals. In this research, we propose a novel multiscale analysis method called multiscale increment entropy (MIE), which integrates incremental entropy (IncrEn) and multiscale analysis. MIE inherits the nature of IncrEn, which considers the fluctuation directions and amplitude of a time series. Experiments on both synthetic and real-world signals indicate that MIE performs better than popular approaches as a complexity index. On each temporal scale, MIE corroborates the complexity-loss theory of ageing and disease well. Furthermore, it reliably discriminates either between the EEG time series and heartbeat intervals of healthy subjects and patients or between the oxygen saturation variability of young and elderly, while commonly used algorithms do not perform well in the above cases. MIE requires less computational time compared to several popular approaches. It also has lower variations and is always defined across scales, even for short time series. These merits make it suitable for analysing unknown physiological time series.

1. Introduction

Complex physiological systems are composed of numerous interconnected structural units. They are often controlled by complex regulatory feedback loops across multiple timescales [1]. The output signals of physiological systems frequently exhibit complex fluctuations, which not only indicate changes in physiological state and/or behaviour but also imply many unconscious outputs of physiological systems. The statistical and dynamic features of these signals can provide information about the early signs of abrupt changes in the system state, health and medical status, and intrinsic characteristics of underlying physiological control mechanisms [2]. It has been proven that the physiological signals of healthy subjects exhibit long-range (fractal) correlations [1]. Long-range correlations and physiological complexity break down with ageing and disease because of degrading normal physiologic control mechanisms that govern healthy functions [1]. To reveal and quantify the mechanisms behind physiological signals, researchers have employed various measures derived from the complexity

* Corresponding author at: College of IoT Engineering, Hohai University, Changzhou 213022, PR China.
E-mail addresses: wangxue@cczu.edu.cn (X. Wang), xfliu@hhu.edu.cn (X. Liu), w.pang@hw.ac.uk (W. Pang), jiangam@hhuc.edu.cn (A. Jiang).

https://doi.org/10.1016/j.ins.2021.11.072
0020-0255/

theory, such as entropy [3–10]. However, entropy-based measures, such as approximate entropy (ApEn) [11] and sample entropy (SampEn) [12], yield higher values for the cardiac interbeat intervals of patients with atrial fibrillation compared to those of healthy individuals. Thus, these entropy metrics are not compatible with the fact that the complexity of the physiological signals decreases with disease and increasing of age. ApEn and SampEn are generally used to measure irregularity in a time series to characterise the physiological complexity. However, neither of them correctly reflect dynamic changes within physiological time series [1,13] because it has been proven that there is no direct correlation between irregularity and physiological complexity [1,14]. Consequently, multiscale entropy based on sample entropy (MSE) [14] was proposed to alleviate this deficiency. MSE provides a multiscale idea that probes the long-correlations of physiological signals to ensure the compatibility between the measured complexity and complexity-loss theory of disease and ageing [15,13].

MSE extends SampEn to multiple time scales by calculating the SampEn values for each coarse-grained time series. Thus, the performance of the MSE was mainly determined by SampEn. There exist several issues with MSE: (1) For many physiological signals, MSE coincides with the complexity-loss theory of ageing and disease only at partial scales, such as cardiac interbeat intervals time series [13], electroencephalogram (EEG) signals [16–19], and pulse wave velocity data [20]. This can lead to the MSE values from physiological signals interlocking under different conditions, means that the MSE is not consistent over different scales. Thus, the guidelines state that one time series is considered more complex than the other, namely, the SampEn values of the former are higher than those of the latter for majority scales. It is challenging to analyse the complexity of unknown and diverse physiological signals. This hinders the application of MSE in real-world cases. This is partially because the description of the signal structure adopted by SampEn is not comprehensive enough. (2) MSE reduces the accuracy of entropy estimation and is often undefined as the data length becomes shorter with an increase in scale [21–23]. This becomes much worse when dealing with short physiological time series [24]. This is attributed to the inherent limitations of sample entropy, which are sensitive to parameters of short signals [25]. (3) The computational efficiency of MSE is relatively poor because there exist two nested loops when calculating SampEn [26].

To alleviate the above issues of MSE, many variants of the traditional MSE method, such as composite multiscale entropy (CMSE)[21] and refined composite multiscale entropy (RCMSE)[22], were proposed. In the classical MSE method, there is only one coarse-grained time series derived from a non-overlapping coarse-grained procedure at scale τ. However, the number of coarse-grained time series is τ at scale τ in the CMSE method, and the sliding windows of all coarse-grained procedures overlap. The mean value of τ SampEn values for all coarse-grained time series is defined as the CMSE value at the scale τ to improve the multiscale entropy accuracy. However, this leads to a poorer computational efficiency for CMSE compared to MSE, which increases the probability of inducing undefined entropy. The RCMSE is an improvement of the CMSE using the total number of template vector matching pairs of τ coarse-grained time series to replace the number of template vector matching pairs of each coarse-grained time series to calculate the negative natural logarithm, which reduces the undefined problem regarding short physiological time series. However, CMSE and RCMSE are still based on SampEn; thus, the first issue remains unsolved. In addition, a variety of entropy measures have been developed for the multiscale complexity analysis of biological signals. For example, multiscale permutation entropy (MPE) [27] calculates the entropy values of coarse-grained time series based on permutation entropy (PE)[28], which is a symbolic dynamic measure based on the natural ordinal pattern of a time series that is computationally effective [28]. However, MPE, though fast, does not fulfil the concept of physiological complexity [29]. This may be because PE ignores the changes in the magnitude of adjacent elements in a time series. Recently, the refined composite multiscale dispersion entropy (RCMDE) [26] has been proposed, which significantly improves the computational efficiency, stability, and discrimination ability compared to traditional MSE and its variants (CMSE and RCMSE) for the complexity analysis of physiological signals. However, RCMDE still has the problem of being inconsistent with the complexity-loss theory of disease and ageing at some scales [30]. This may be because RCMDE only considers the fluctuation amplitude in the time series and does not completely consider the time series fluctuation.

To alleviate these deficiencies of MSE, we propose a novel method called multiscale increment entropy (MIE) to better characterise the physiological complexity over multiple time scales. The entropy calculation of the coarse-grained time series in MIE is based on incremental entropy (IncrEn) [31], which was proposed by Liu *et.al*. IncrEn not only naturally encodes the rank order of a time series in the form of symbol sequences but also quantifies the magnitude of the variation between adjacent elements. Thus, IncrEn can better characterise the structural information in physiological time series compared to SampEn and PE [31]. In this study, the performance of MIE was assessed and compared to RCMDE and MSE in terms of their consistency with the complexity-loss theory, accuracy, computational efficiency, and undefined entropy problem.

The remainder of this paper is organised as follows: Section 2 reviews MSE, RCMSE, RCMDE, and refined composite multiscale permutation entropy (RCMPE), then presents MIE. The time series used for the evaluation employed in this study are introduced in Section 3. We assess the performance of MIE and compare it to the related methods in Section 4. Finally, the discussion and conclusions are presented in Sections 5 and 6, respectively.

2. Methods

In this section, the theoretical background for MSE, RCMDE, and RCMPE cited in this research are briefly introduced, and the proposed MIE method is presented in detail.

2.1. Multiscale entropy based SampEn and its variants

Multiscale entropy analyses the complexity of time series on different time scales. Thus, MSE consists of two producers: 1) coarse-grained producers, as shown in Fig. 1, for a one-dimensional discrete raw time series $\mathbf{u} = \{u(i), 1 \leqslant i \leqslant L\}$, the consecutive coarse-grained time series $\mathbf{x}^{(\tau)} = \left\{x_j^{(\tau)}\right\}$ is constructed by averaging the data points within each non-overlapping window of length τ according to the following equation:

$$x_j^{(\tau)} = \frac{1}{\tau}\sum_{i=(j-1)\tau+1}^{j\tau} u_i, 1 \leqslant j \leqslant \lfloor\frac{L}{\tau}\rfloor = N, \tag{1}$$

where τ is the scale factor and N is the length of the coarse-grained time series with respect to τ, which is equal to the floor of $\frac{L}{\tau}$. 2) calculate the SampEn value of the consecutive coarse-grained time series $\mathbf{x}^{(\tau)}$ as shown below:

$$MSE(\mathbf{u}, \tau, m, r) = SampEn(\mathbf{x}^{(\tau)}, m, r) = -\ln\frac{n_{m+1}}{n_m}, \tag{2}$$

where r is the similarity criterion and n_m and n_{m+1} represent the number of m-dimensional and $(m+1)$-dimensional template vector matching pairs derived from the time series $\mathbf{x}^{(\tau)}$ with the distance between vector pairs less than r, respectively. The parameter r for each coarse-grained time series remains constant and is equal to the value on the first scale (usually $0.15 * SD$ of the original signal).

With an increase in scale, the accuracy of MSE decreases. MSE often induces undefined entropy; thus, a RCMSE method is proposed in this study. RCMSE improves the coarse-grained process such that; for a scale τ, there are τ different coarse-grained time series, and the k^{th} coarse-grained time series $\mathbf{x}_k^{(\tau)} = \left\{x_{k,1}^{(\tau)}, x_{k,2}^{(\tau)}, \ldots\right\}$ is stated as follows:

$$x_{k,j}^{(\tau)} = \frac{1}{\tau}\sum_{i=(j-1)\tau+k}^{k+j\tau-1} u_i, 1 \leqslant j \leqslant \lfloor\frac{L}{\tau}\rfloor = N, 1 \leqslant k \leqslant \tau. \tag{3}$$

Then RCMSE is defined as stated below:

$$RCMSE(\mathbf{u}, \tau, m, r) = -\ln\left(\frac{\overline{n}_{m+1}^{(\tau)}}{\overline{n}_m^{(\tau)}}\right), \tag{4}$$

where $\overline{n}_{m+1}^{(\tau)} = \frac{1}{\tau}\sum_{k=1}^{\tau} n_{k\ m+1}^{(\tau)}, \overline{n}_m^{(\tau)} = \frac{1}{\tau}\sum_{k=1}^{\tau} n_{k\ m}^{(\tau)}$. $n_{k\ m}^{(\tau)}$ and $n_{k\ m+1}^{(\tau)}$ refer to the number of matches for m-dimensional and $(m+1)$-dimensional matched vector pairs derived from the time series $\mathbf{x}_k^{(\tau)}$ with vector pair distances less than r, respectively.

2.2. Refined composite multiscale dispersion entropy

For RCMDE, the entropy of the coarse-grained time series is calculated using dispersion entropy (DisEn) [33]. There are τ different coarse-grained time series at scale τ according to Eq. (3). DisEn maps the coarse-grained time series $\mathbf{x}_k^{(\tau)}$ into $\mathbf{y} = \{y_1, y_2, \cdots, y_N\}$ using the normal cumulative distribution function as follows:

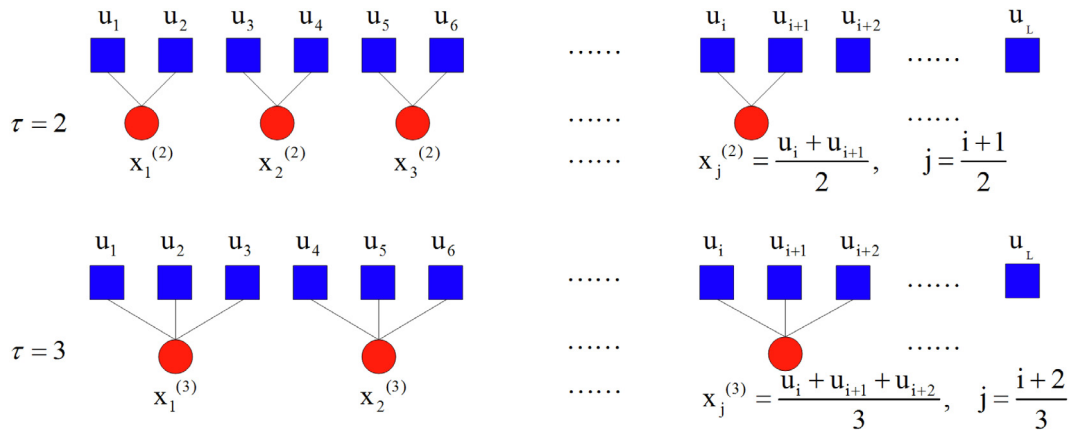

Fig. 1. Schematic illustration of the coarse-grained procedure. Modified from reference [32].

$$y_j = \frac{1}{\delta\sqrt{2\pi}} \int_{-\infty}^{x_{kj}^{(\tau)}} e^{\frac{-(t-\mu)^2}{2\delta^2}}, \tag{5}$$

where δ and μ are the SD and mean of the time series $\mathbf{x}_k^{(\tau)}$, respectively. Then, $\mathbf{y}$ is mapped into the classified time series $\mathbf{z}, z_j^c = round(c.y_j + 0.5)$, where c denotes the number of classes. $\mathbf{z}$ is divided into $N - m + 1$ vectors with m elements, and each vector is mapped into a dispersion pattern. The number of possible dispersion patterns that can be assigned to each vector is c^m; then, we can calculate the relative frequency $p_{k,\pi}$ of each dispersion pattern in the coarse-grained time series $\mathbf{x}_k^{(\tau)}$. Moreover, the DisEn value of the coarse-grained time series $\mathbf{x}_k^{(\tau)}$ is calculated as follows:

$$DisEn(\mathbf{x}_k{}^{(\tau)}, m, c) = -\sum_{\pi=1}^{c^m} p_{k,\pi} \ln p_{k,\pi}. \tag{6}$$

RCMDE of the raw time series $\mathbf{u}$ is defined as follows:

$$RCMDE(\mathbf{u}, m, c, \tau) = -\sum_{\pi=1}^{c^m} \overline{p_\pi} \ln \overline{p_\pi}, \tag{7}$$

where $\overline{p_\pi} = \frac{1}{\tau}\sum_{k=1}^{\tau} p_{k,\pi}$ is the relative frequency of the π^{th} dispersion pattern in all coarse-grained series on scale τ.

2.3. Refined composite multiscale permutation entropy

The calculation of the RCMPE is similar to that of the RCMDE. For scale τ, we first construct τ different coarse-grained time series using Eq. (3). Then, m-dimensional vectors $\mathbf{x}_{\mathbf{k},\mathbf{d}} = \left[\mathbf{x}_{\mathbf{k},\mathbf{j}}, \mathbf{x}_{\mathbf{k},\mathbf{j}+\mathbf{d}}, \ldots, \mathbf{x}_{\mathbf{k},\mathbf{j}+(\mathbf{m}-\mathbf{1})\mathbf{d}}\right]$ derived from the coarse-grained time series $\mathbf{x}_\mathbf{k}^{(\tau)}$ are constructed, where d is the delay parameter. The number of possible permutation patterns of an m-dimensional vectors is equal to $m!$. Therefore, the RCMPE is defined as:

$$RCMPE(\mathbf{u}, m, d, \tau) = -\sum_{\pi=1}^{m!} \overline{p_\pi} \ln \overline{p_\pi}, \tag{8}$$

where $\overline{p_\pi} = \frac{1}{\tau}\sum_{k=1}^{\tau} p_{k,\pi}$ is the relative frequency of the permutation pattern π in all coarse-grained series on scale τ. $p_{k,\pi}$ represents the relative frequency of the π^{th} permutation pattern in the coarse-grained time series $\mathbf{x}_k^{(\tau)}$.

2.4. The proposed multiscale increment entropy

Our proposed MIE comprises both the advantages of MSE [14] and IncrEn [31], which is more than a simple combination of coarse-grained processes [14] and IncrEn. For a one-dimensional discrete time series $\mathbf{u} = \{u(i), 1 \leqslant i \leqslant L\}$, the flow chart of the MIE is shown in Fig. 2. There are mainly two steps in MIE: the coarse-grained time series generation procedure and IncrEn calculation procedure. The IncrEn calculation procedure is composed of five steps. The detailed calculation steps of the MIE are as follows:

i) Generate a consecutive coarse-grained time series $\left\{x_j^{(\tau)}, 1 \leqslant j \leqslant N\right\}$ according to Eq. (3).

ii) Calculate the IncrEn value for a coarse-grained time series $\mathbf{x}^{(\tau)}$ as follows:

a) Construct an increment series $\mathbf{v} = \{v(j), 1 \leqslant j \leqslant N-1\}$, where $v(j) = x_{j+1}^{(\tau)} - x_j^{(\tau)}$.

b) Divide the increment series into $N - m$ increment vectors, $V(k) = [v(k), v(k+1), \ldots, v(k+m-1)], 1 \leqslant k \leqslant N-m$, where m denotes the number of embedding dimensions.

c) Map each element of the increment vector into a word consisting of two elements: the sign(s) and size(q). The sign indicates the direction of volatility between the corresponding neighbouring elements in the coarse-grained time series. It takes the values of 1, 0, or -1, indicating an increase, no change, or decline, respectively. The size that describes the magnitude of the variation between these adjacent elements depends on the resolution parameter R. Each increment vector is then mapped to a pattern vector with $2m$ elements. Thus, given m and R, each increment vector has $(2R+1)^m$ variant patterns. For the increment vector $V(k)$, the sign s_k of $v(k)$ is calculated as follows:

$$s_k = sgn(v(k)), \tag{9}$$

and q_k is the size of $v(k)$, calculated as stated below:

$$q_k = \begin{cases} 0, & step = 0 \\ \min\left(R, \lfloor \frac{|v(k)| \times R}{step} \rfloor\right), & step \neq 0 \end{cases} \tag{10}$$

where *step* in Eq. 10 is the SD of the increment series constructed from the coarse-grained time series $\mathbf{x}^{(1)} = \{u(i), 1 \leqslant i \leqslant L\}$. Note that R and *step* remain constant for all scale factors.

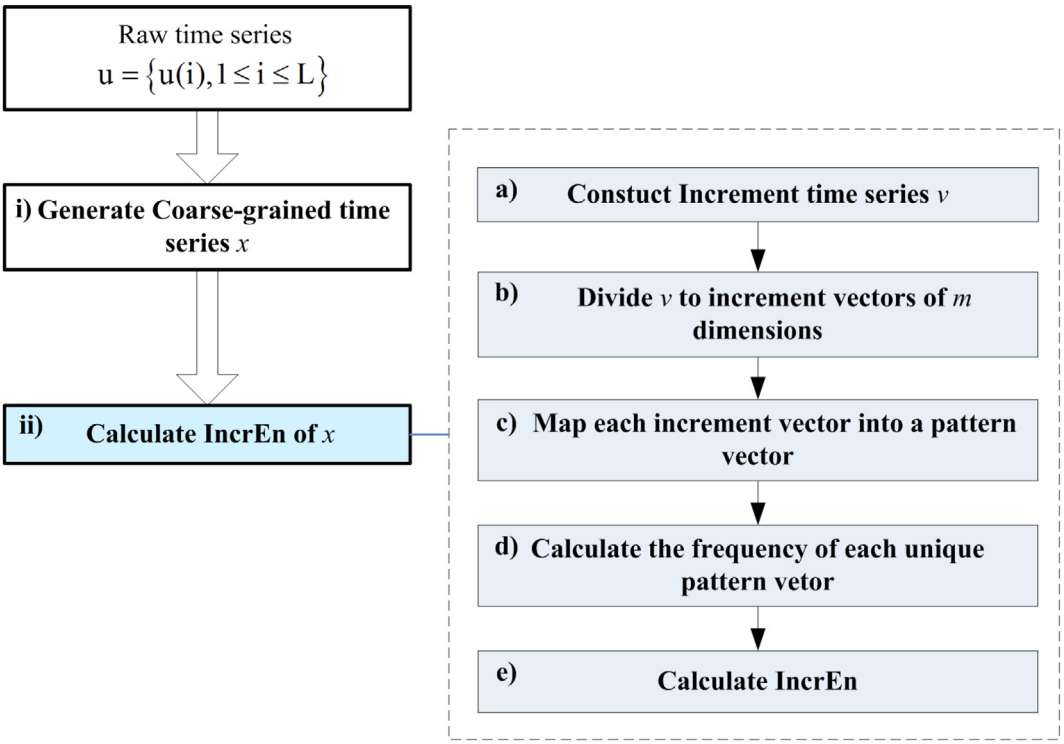

Fig. 2. The flow chart of MIE.

d) Define the relative frequency of each unique pattern vector as follows:

$$P(w_n) = \frac{Q(w_n)}{N-m}, \tag{11}$$

where w_n denotes the n^{th} unique pattern vector, and $Q(w_n)$ is the total number of instances for the n^{th} unique pattern vector.

e) Define the MIE value at scale τ as stated below:

$$\begin{aligned} MIE(\mathbf{u}, m, R, \tau) = & \ IncrEn\left(\mathbf{x}^{(\tau)}, m, R\right) \\ & = -\tfrac{1}{m-1}\sum n = 1^{(2R+1)^m} P(w_n)\log P(w_n). \end{aligned} \tag{12}$$

In the abovementioned equation, $m-1$ is a normalisation factor, and MIE is bounded within $\left[0, \frac{m\log(2R+1)}{(m-1)}\right]$.

The complete MIE algorithm is illustrated using the example shown in Fig. 3. The original time series is $\{u(i)\}_{i=1}^{L=12}$whose data length L equals 12. $\{x(j)^{\tau}\}_{j=1}^{N=6}$is the coarse-grained time series with a data length of 6 and scale factor τ of 2. The parameters of IncrEn are set to $m = 2$ and $R = 4$, and IncrEn is calculated following Step ii. We construct an increment time series $\{v(j)\}_{j=1}^{5}$; then, map the four increment vectors to the four pattern vectors. There are four unique patterns, each with one instance. According to Eqs. (11) and (12), MIE equals 2.

3. Time series used for evaluation

To carry out our investigation, both a simulated time series with known entropy qualities and real-world experimental time series are used in this study.

3.1. Simulated time series

The simulated time series consist of $1/f$ noise, white noise, and Brownian noise. The $1/f$ noise has an outstanding fractal feature. It exists in many physiological signals that exhibit complex dynamics with long-range correlations. The completely uncorrelated (white) noise and random walk (Brownian noise) are the two types of dynamical end-states that can be ultimately reached by damaged physiological systems [1]. Thus, we assess the effectiveness of MIE based on the complexity analysis of the simulated time series with these three types of noise. There are three types of time series simulated each com-

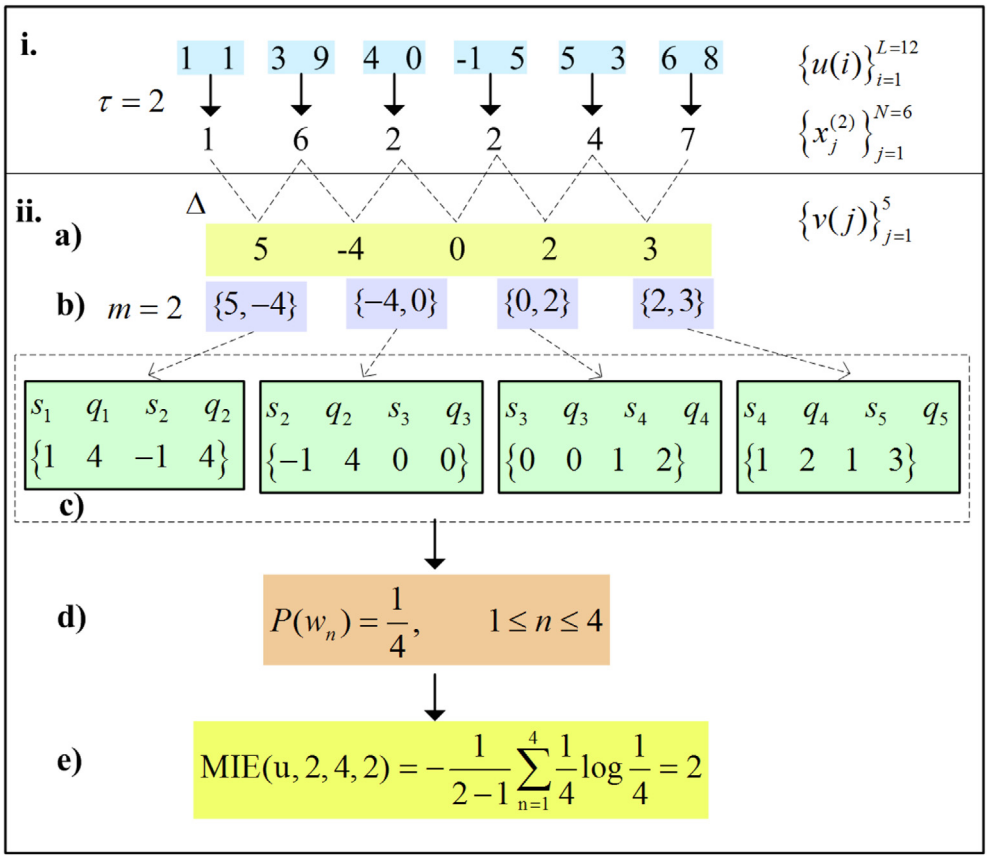

Fig. 3. Schematic diagrams of MIE illustrated by an example. i). An example of a coarse-grained procedure (scale factor τ equals 2). ii). The core IncrEn calculation for the coarse-grained time series that takes the embedding dimension $m = 2$ and resolution parameter $R = 4$.

prising 30 individual time series. Each simulated time series contains 10,000 samples. We produce a Gaussian distributed white noise time series with zero mean and unit variance and an ordinary Brownian noise time series. $1/f$ noise time series are produced based on the feature that the power spectrum density of a $1/f$ noise is inversely proportional to the frequency.

3.2. Real-world time series

Three physiological datasets were used to investigate the performance of MIE. The first time series dataset comprises EEG data derived from healthy subjects and patients with epilepsy. The second dataset, corresponding to different health states, consists of cardiac interbeat intervals (RRs) from subjects with three different physiological states. The third dataset consists of the oxygen saturation variability (OSV) time series sampled from individuals of different ages. The basic information of the three datasets are summarised in Table 1. The details of each database are provided below.

- Datasets derived from healthy subjects and patients

  (1) The EEG datasets are obtained from the Department of Epileptology, Bonn University, Germany (http://epileptologie-bonn.de/cms/front_content.php?idcat=193&lang=3&changelang=3) [34]. The site provides five datasets, A to E. Only datasets A and D were employed in this study. Dataset A consists of surface EEG recordings from healthy subjects.

Table 1
The basic information of the real-world datasets used in this study.

Datasets	Feature		Note
	The number of the time series	Data length	
EEG	5 healthy and 5 epileptic	4,700	health vs. epilepsy during seizure-free intervals
RR	18 healthy, 84 atrial fibrillation, and 15 congestive heart failure	20,000	health vs. the two different pathological states
OSV	20 young and 20 elderly	3,500	healthy young vs. healthy elderly

Dataset D contains intracranial EEG signals recorded from the epileptogenic zone of five subjects with epilepsy during seizure-free intervals. Each dataset contains 100 files, and each file contains 23.6 seconds of EEG data. All EEG signals were sampled at 173.61 Hz using a 128-channel amplifier system with an average common reference and band-pass filtered at 0.53 $\sim$ 40 Hz. Consequently, each file contained approximately 4097 data points.

The RR datasets are derived from subjects with normal sinus rhythm (NSR), congestive heart failure (CHF), and atrial fibrillation (AF). These three datasets are available from the MIT-BIH NSR database (https://physionet.org/content/nsrdb/1.0.0/), BIDMC CHF database (https://physionet.org/content/chfdb/1.0.0/), and long-term AF database (https://physionet.org/content/ltafdb/1.0.0/), respectively [35]. Subjects from the NSR database had no significant arrhythmias and included 5 men aged 26–45 years and 13 women aged 20–50 years. All signals were sampled at 128 Hz. The CHF database included 15 subjects (11 men aged 22–71 years and four women aged 54–63 years) with congestive heart failure (NYHA class 3$\sim$4). Each time series was sampled at 250 samples/s. The AF database consisted of 84 atrial fibrillation recordings sampled at 250 samples per second. The subjects had either paroxysmal or sustained AF. Each time series in the RR datasets contained 20,000 points.

- Datasets derived from healthy young and elderly individuals

(3) The OSV datasets consist of 20 time series from healthy young subjects (mean age: 21.0; SD: 1.36 years) and 15 time series from healthy elderly individuals (mean age: 50.3; SD: 10.7 years). All young subjects were younger than 35 years of age. The datasets were obtained from the OSV database (https://physionet.org/physiobank/database/osv/) [36,35]. To reflect the true SpO_2 variation, the resolution was reduced from 1k/s to 1/s. Each time series of the OSV datasets contained 3,500 points.

4. Experiments and results

For all methods, all parameters of the algorithms are set to the recommended values. The time delay is set to 1, the embedding dimension $m = 2$ in MSE and RCMDE, and $m = 5$ in RCMPE [37]. The parameter r equals 0.15 of the original signal SD in MSE [12]. The number of classes c is set to six in the RCMDE [26]. The simulation is performed using a PC with an Intel (R) core (TM) i7-5500U CPU working at 2.4 GHz and 4 GB of RAM with MatLab R2014a.

4.1. Experiments on simulated data

We used the simulated data to evaluate the validation, stability, and computational efficiency of the MIE.

The validation of MSE, RCMDE, RCMPE, and MIE in mining the complexity of the simulated signals is presented in Fig. 4. The results obtained by using MSE and RCMDE over white noise time series and $1/f$ noise time series show that, for $\tau \leq 3$, MSE and RCMDE values of the white noise are higher than those of the $1/f$ noise. However, a higher value of entropy is assigned to the $1/f$ time series compared to the white noise time series for scale $\tau > 3$. (Figs. 4(a) and (b)). In contrast, the MIE value of the $1/f$ noise remains higher than that of the white noise. However, the RCMPE values of the white noise remain almost constant for all scales. It yields lower values for $1/f$ noise than those for white noise at any scale, which con-

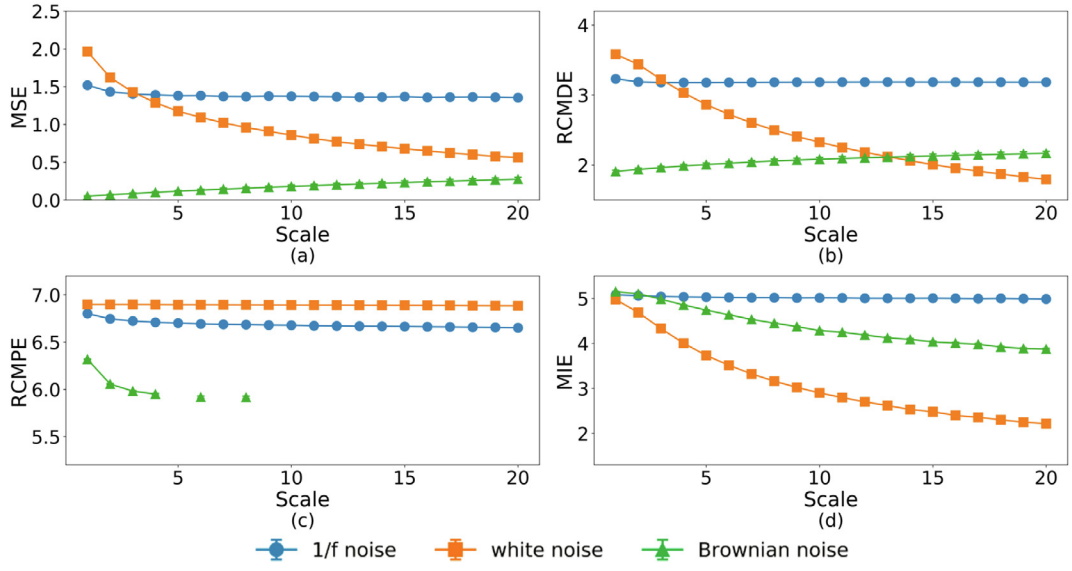

Fig. 4. The mean values for the MSE (a), RCMDE (b), RCMPE (c), and MIE(d) results computed from 30 different simulated $1/f$ noise, white noise, and Brownian noise signals, each of which is composed of 10,000 points. For MIE, $m = 2, R = 2$.

tradicts the fact that $1/f$ noise contains more complex structures compared to white noise across multiple time scales [14]. The values of MSE and RCMDE for the Brownian noise time series slightly increase with an increase in scale and are lower than those of the $1/f$ noise time series at each scale. The MIE curve of the Brownian noise time series decreases monotonically with an increase in scale. MIE yields lower values for the Brownian noise time series compared to the $1/f$ noise time series at most scales, except at scales less than 3. However, MPE is undefined for the Brownian noise time series at most scales. Thus, no further investigation is performed regarding RCMPE.

Table 2 shows the stability of MIE, MSE, and RCMDE. We use the coefficient of variation (CV), which is defined as the SD divided by the mean. The results reported in Table 2 demonstrate that the CV values of RCMDE and MIE are less than that of MSE for scale $\tau = 10$. Moreover, for MIE, the CV values of the $1/f$ and Brownian noises are the smallest.

Table 3 displays the runtime data for MSE, RCMDE, and MIE algorithms using 30 different $1/f$ noise time series with different data lengths. The runtime of MIE is significantly faster than those of MSE and RCMDE, especially for long signals. The time for calculating MSE increases notably with increasing time series lengths but for MIE this is not the case.

Table 2
CV values of the MSE, RCMDE, and MIE algorithms from the analyses for $1/f$ noise, white noise, and Brownian noise (scale factor $\tau = 10$). For each time series type, the smallest CV value is reported in bold.

Time Series	MSE	RCMDE	MIE
$1/f$ noise	0.0325	0.0099	**0.0058**
white noise	0.0297	**0.0128**	0.0197
brownian noise	0.5501	0.0715	**0.0166**

Table 3
The runtime data for the MSE, RCMDE and MIE algorithms used to analyse 30 different $1/f$ noise time series with different data length ($m = 2$). For each data length, the shortest runtime is indicated in bold.

Data Length	MSE	RCMDE	MIE
10,000	518.01 s	66.44 s	**23.28 s**
5,000	98.95 s	33.98 s	**12.96 s**
2,000	20.12 s	14.65 s	**7.2 s**
1,000	7.99 s	8.15 s	**5.04 s**

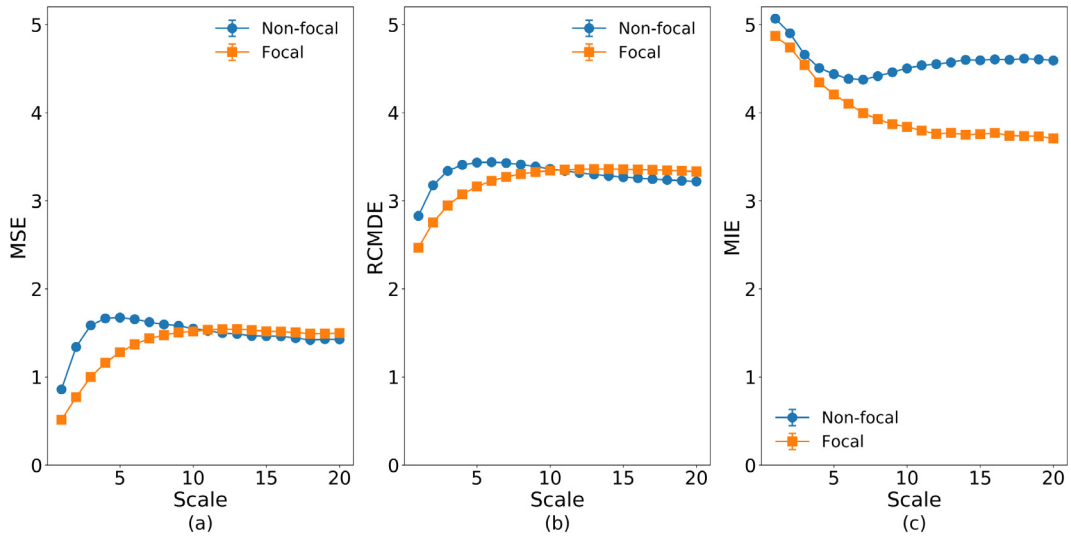

Fig. 5. The mean value and standard errors for the mean of MSE (a), RCMDE (b), MIE (c) using the EEG time series for healthy subjects (Non-focal) and epileptic patients (Focal). For MIE, $m = 2, R = 2$.

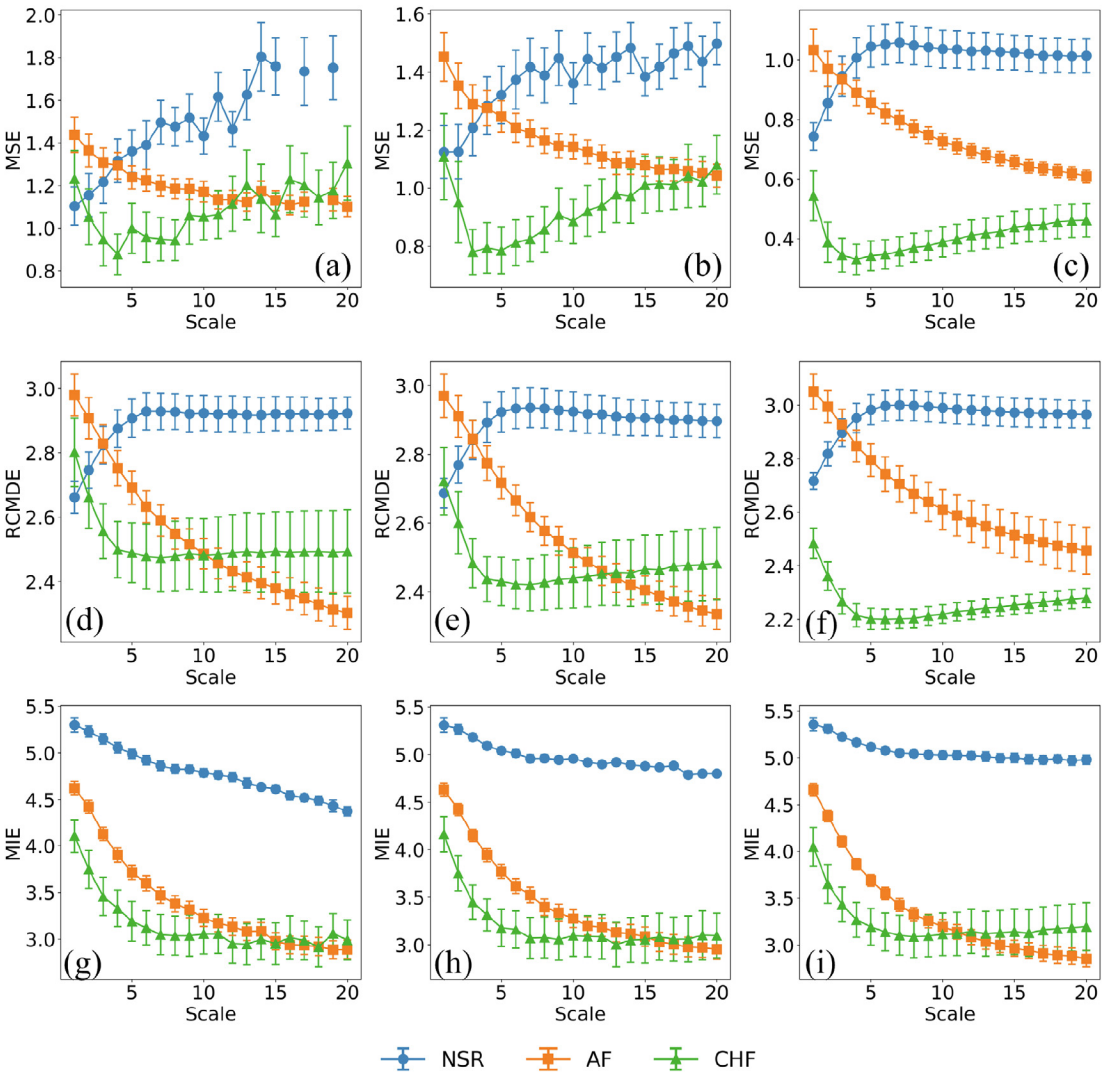

Fig. 6. The mean and standard errors of MSE, RCMDE, MIE analyses for the cardiac interbeat intervals of healthy subjects (NSR), subjects with heart failure (CHF), and subjects with AF group. The first row shows the results of MSE (data length equals 1,000 points (a), 2,000 points (b), and 20,000 points [c]). The second row shows the results of RCMDE (the data length is 1,000 (d), 2,000 (e), and 20,000 (f)). The third row shows the results of MIE (the data length is 1,000 (g), 2,000 (h), and 20,000 (i)). For MIE, $m = 2, R = 2$.

4.2. Experiments on real physiological data

In this section, we employ our proposed method for analysing different types of physiological signals to detect different pathological states and ages.

The analysis results of the three methods over the EEG time series of healthy subjects and interictal EEG time series of epileptic patients are shown in Fig. 5. At each scale, MIE yields higher values for non-focal subject EEG time series compared to interictal EEG time series from epileptic focal subjects. However, the analysis results of MSE and RCMDE over the two types of time series are inconsistent across scales. With an increase in scale, the curves of MSE and RCMDE over the EEG time series of non-focal subjects and epileptic focal patients intersect. They both yield higher values for non-focal subjects compared to epileptic focal subjects for scales less than 9; whereas, for $\tau \geqslant 10$, the MSE and RCMDE values of healthy EEG time series are lower compared to epileptic patients interictal EEG time series.

The results depicted in Fig. 6 reveal that: (1) MIE enables a clearer and consistent distinction between the interval interbeat time series (NSR) of healthy individuals and time series of pathologic subjects with heart failure (CHF) or AF at all scales (Fig. 6(i)). (2) The MSE and RCMDE yield similar results. The identification results based on the MSE and RCMDE change over varying scales. They yield lower entropy values for the healthy subject time series compared to pathologic time series from the AF subject for scales less than 3 (Figs. 6(c) and (f)). With an increase in scale, the entropy values of the healthy subjects

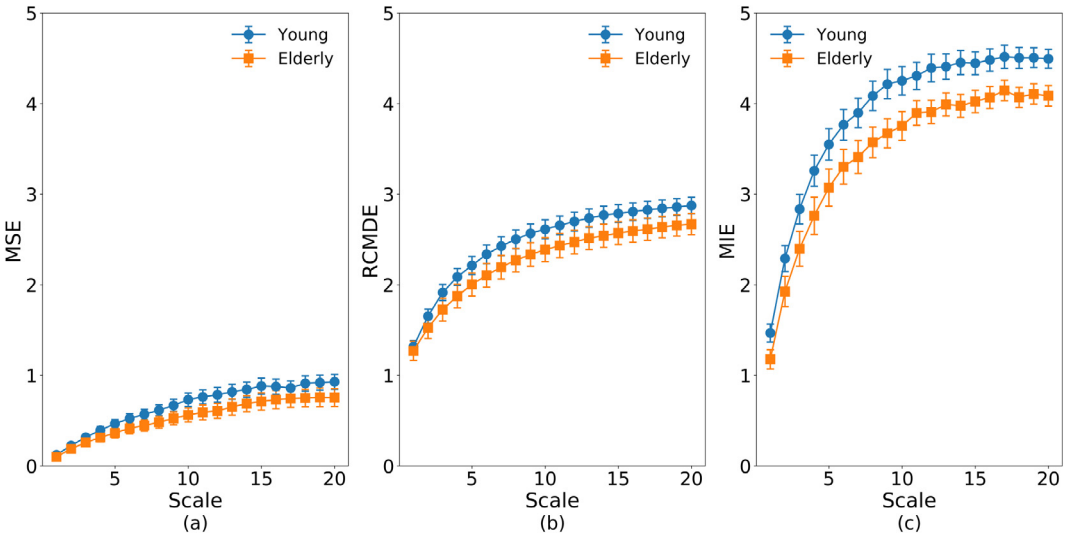

Fig. 7. The mean value and standard errors for the mean of MSE (a), RCMDE (b), MIE (c) using the OSV time series for 20 young individuals and 16 elderly subjects. For MIE, $m = 2, R = 2$.

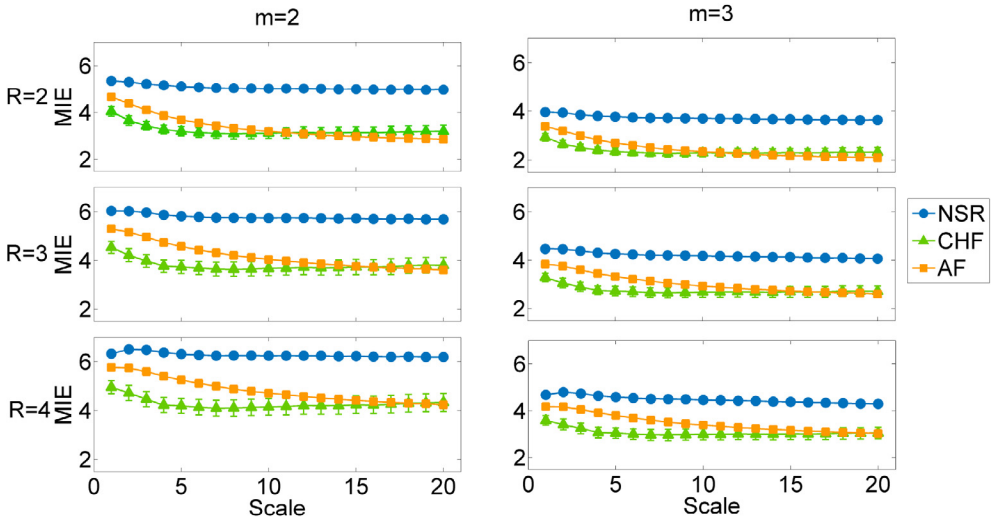

Fig. 8. The mean and standard errors of MIE analysis for the cardiac interbeat intervals of healthy subjects (NSR), subjects with heart failure (CHF), and subjects with AF group with different m and R values. The first row shows the MIE values with $R = 2$. The second row shows the results of MIE with $R = 3$. The third row shows the results of MIE with $R = 4$. The left column refers to $m = 2$ and right column refers to $m = 3$. The data length for all time series is 20,000.

are higher than those of the pathologic subjects. (3) The MSE, RCMDE, and MIE curve profiles of the heart failure time series (CHF) and atrial fibrillation time series (AF) significantly decrease on smaller scales. Instead, for a healthy interbeat intervals time series, the MSE and RCMDE values increase on a very small scale (≤ 5); then, remain approximately invariant with an increase in scale. The MIE curve profile of the healthy interbeat intervals time series drops slightly; then, remains approximately invariant with an increase in scale.

The results shown in Fig. 7 reveal the following: (1) MIE yields higher values for young individuals compared to elderly subjects. (2) MSE and RCMDE lead to slight differences for the two OSV groups, while MIE over the young and elderly OSV time series shows obvious differences and consistent identification results across scales. (3) The MSE, RCMDE, and MIE curve profiles of the OSV time series gradually increase with an increase in scale, which agrees with previous studies [36].

In addition, we investigated the dependence on the data length of MSE, RCMDE, and MIE using heartbeat time series derived from healthy subjects and patients. The results presented in Fig. 6 are summarised as follows: (1) The identification results of MIE are generally consistent for the three time series types with varying data lengths. However, for MSE and RCMDE, the difference between the heart failure time series (CHF) and atrial fibrillation time series (AF) or healthy time ser-

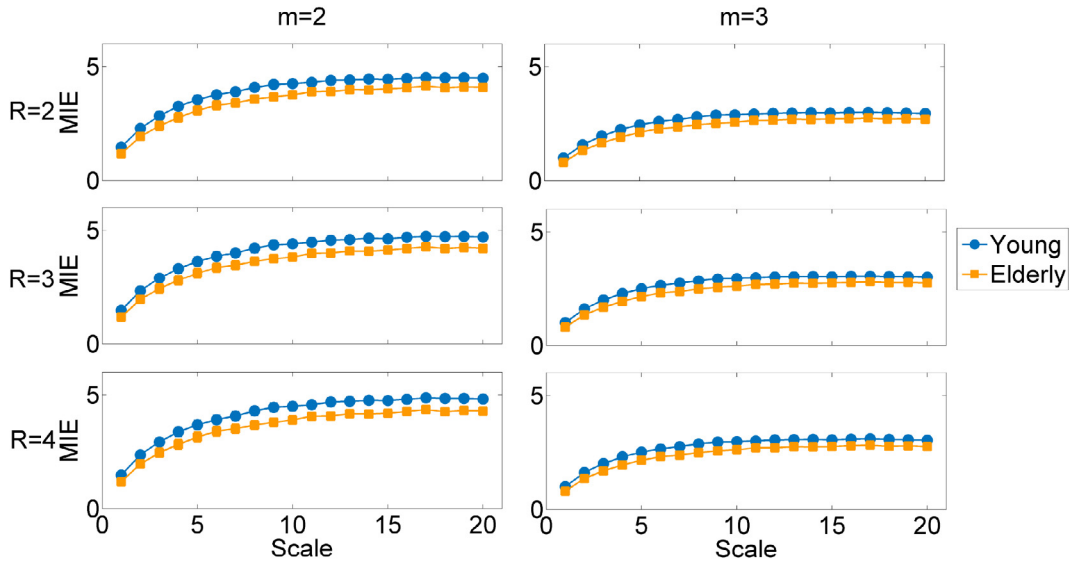

Fig. 9. The mean and standard errors of MIE analysis for the young and elderly OSV time series with the resolution R ranging from 2 to 4 and dimension parameter m within the interval $[2, 3]$. The 1st row shows the MIE values with $R = 2$. The middle row shows the MIE results with $R = 3$. The 3rd row shows the MIE results with $R = 4$. The left column refers to $m = 2$ and right column refers to $m = 3$.

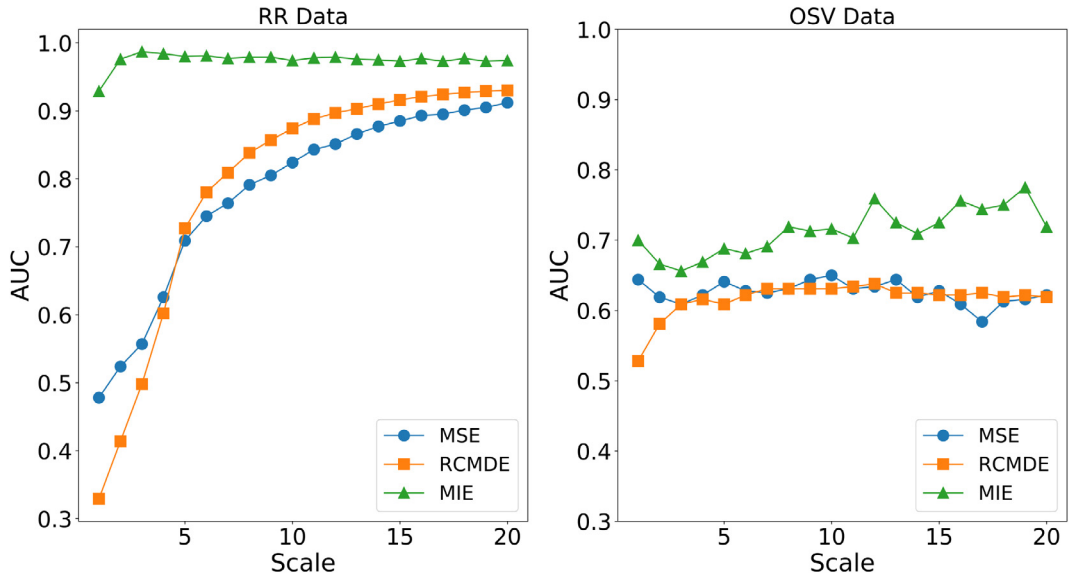

Fig. 10. AUC values regarding MSE, RCMDE, MIE features of the RR and OSV datasets at scales ranging from 1 to 20.

ies (NSR) is not consistent (Figs. 6(a)∼(f)) for different data lengths. (2) MSE induces undefined entropy at large scales ($s \geqslant 15$) for data length $= 1,000$ (Fig. 6(a)). In contrast, MIE and RCMDE are defined at each scale in shorter time series. (3) The MSE values become unstable and fluctuate with an increase in scale for data length $\leqslant 2,000$. This issue is not obvious for the MIE and RCMDE.

The effects of the dimension parameter m and resolution parameter R on the MIE are also investigated over the RR and OSV datasets. According to an appropriate choice of the parameters of IncrEn [38], m is set to either 2 or 3, and the values of R range from 2 to 4 in increments of one. The results shown in Fig. 8 and Fig. 9 demonstrate that entropy values decrease with increasing m and R, which coincides with the effect of m and R on IncrEn. The difference between the two groups becomes more obvious for larger R or smaller m because MIE can identify more patterns of time series in such cases. MIE exhibits better relative consistency with $m = 2, m = 3$ and, $2 \leqslant R \leqslant 4$.

Table 4
One-way ANOVA results for the MSE, RCMDE and MIE values of each experimental dataset with a scale range of 1–20 ($\alpha \leqslant 0.05$).

Scale	*p*-values for Healthy vs. Patient RR time series			*p*-values for Young vs. Elderly OSV time series		
	MSE	RCMDE	MIE	MSE	RCMDE	MIE
1	0.004	0.000	0.000	0.287	0.696	0.054
2	0.000	0.000	0.000	0.340	0.351	0.122
3	0.000	0.000	0.000	0.286	0.213	0.115
4	0.000	0.000	0.000	0.205	0.182	0.091
5	0.000	0.000	0.000	0.166	0.198	0.066
6	0.000	0.000	0.000	0.186	0.167	0.092
7	0.000	0.000	0.000	0.156	0.170	0.080
8	0.000	0.000	0.000	0.152	0.169	0.043
9	0.000	0.000	0.000	0.159	0.164	0.062
10	0.000	0.000	0.000	0.125	0.180	0.041
11	0.000	0.000	0.000	0.145	0.188	0.078
12	0.000	0.000	0.000	0.131	0.174	0.023
13	0.000	0.000	0.000	0.179	0.180	0.046
14	0.000	0.000	0.000	0.213	0.160	0.055
15	0.000	0.000	0.000	0.202	0.178	0.034
16	0.000	0.000	0.000	0.271	0.175	0.012
17	0.000	0.000	0.000	0.356	0.174	0.043
18	0.000	0.000	0.000	0.212	0.177	0.013
19	0.000	0.000	0.000	0.226	0.180	0.007
20	0.000	0.000	0.000	0.179	0.169	0.020

Fig. 10 shows the values for the ROC area under curves (AUC) regarding the MSE, RCMDE, and MIE features of the two experimental datasets with the scale ranging from 1 to 20. Compared to MSE and RCMDE, MIE produces larger AUC values on any scale over both the heartbeat datasets of healthy and patient and OSV datasets. In addition, one-way ANOVA analysis with a least significant difference test is conducted to analyse the statistical significance of the experimental results for MSE, RCMDE, and MIE among different classes of time series in the two physiological signal datasets. The results reported in Table 4 reveal that, *p*-values over healthy and patient groups obtained using MSE, RCMDE, and MIE are less than 0.05 for all scales, which demonstrates that the values of MSE, RCMSE, and MIE are significant for both the healthy heartbeat time series and patient time series. The *p*-values of MIE over young and elderly OSV time series are less than those of MSE and RCMDE. In addition, the *p*-values of MSE and RCMDE are greater than 0.05 for all scales, while most *p*-values of MIE are less than 0.05 for scale $\tau \geqslant 8$, which demonstrates that MIE is the only significant index among the three indices regarding the healthy young and elderly OSV groups.

We also used Fisher's discriminant function to evaluate the performance of these indices to distinguish the recordings of each group. The overall accuracy, sensitivity, and specificity of the different indices were calculated. All statistical tests were performed using SPSS version 22.0.0.0. The overall accuracy, sensitivity, and specificity values of MSE, RCMDE, and MIE are presented in Table 5. The highest accuracy, sensitivity, and specificity of MIE over the healthy and patient RR time series were 94.87%, 100%, and 93.94%, respectively, for scales $\tau = 3$ and $\tau = 4$. While MSE and RCMDE had better identification ability on a large scale, the highest accuracy, sensitivity, and specificity of MSE were $91.45\%, 77.78\%$, and 93.94%, respectively, for $\tau = 20$; while those of RCMDE were $86.32\%, 83.33\%$, and 86.87%, respectively, for $\tau = 15$. The accuracy, sensitivity, and specificity of MSE and RCMDE over healthy and patient RR time series were lower than those of MIE on most scales. MIE over young and elderly OSV time series had 75% higher accuracy, sensitivity, and specificity compared to MSE and RCMDE. In addition, MIE performed better than those derived from a single entropy (IncrEn, $\tau = 1$).

5. Discussions

In this research, the MSE, RCMDE, and MIE are compared in terms of their ability to measure the complexity of physiological time series. A common perspective is that a useful physiological complexity measure should correctly reflect dynamic changes within a time series. Although the analysis results of MIE with the Brownian noise time series and $1/f$ noise time series are inconsistent over all scales, for heart failure time series, which is similar to the Brownian noise time series [39], MIE yields lower values compared to healthy subjects for all scales. The results for other real-world time series demonstrate that MIE supports the fact that the output of healthy systems reveals long-range correlations, which break down with ageing and disease. The long-range correlations in physiological signals of healthy individuals underline the adaptation ability of living systems to ever-changing environments [13]. Instead, the breakdown of long-range correlation properties in disease reflects a reduced ability of integrated physiological responsiveness [1,39], which leads to complexity loss in the time series obtained from patients [13]. Therefore, entropy values, which represent the complexity of physiological time series, should decrease with ageing and disease. In the results obtained from MSE, RCMDE, and the proposed MIE method, only the MIE

Table 5
Classification results for MSE, RCMDE, and MIE algorithms over experimental time series with a scale range of 1–20.

Indices	Scale	Healthy vs. Patient RR time series			Young vs. Elderly OSV time series		
		Acc(%)	Sen(%)	Spe(%)	Acc(%)	Sen(%)	Spe(%)
MSE	1	81.20	50.00	86.87	61.11	55.00	68.75
	2	78.63	44.44	84.85	58.33	50.00	68.75
	3	58.12	50.00	59.60	61.11	50.00	75.00
	4	58.12	55.56	58.59	58.33	50.00	68.75
	5	58.97	55.56	59.60	61.11	50.00	75.00
	6	61.54	61.11	61.62	58.33	50.00	68.75
	7	62.39	61.11	62.63	63.89	55.00	75.00
	8	64.10	66.67	63.64	61.11	55.00	68.75
	9	66.67	66.67	66.67	61.11	50.00	75.00
	10	70.94	66.67	71.72	63.89	65.00	62.50
	11	76.07	72.22	76.77	61.11	55.00	68.75
	12	75.21	66.67	76.77	58.33	55.00	62.50
	13	82.91	72.22	84.85	61.11	60.00	62.50
	14	86.32	77.78	87.88	58.33	60.00	56.25
	15	89.74	77.78	91.92	58.33	55.00	62.50
	16	88.89	77.78	90.91	55.56	55.00	56.25
	17	89.74	77.78	91.92	58.33	60.00	56.25
	18	88.89	77.78	90.91	58.33	55.00	62.50
	19	88.89	77.78	90.91	63.89	65.00	62.50
	20	91.45	77.78	93.94	58.33	60.00	56.25
RCMDE	1	77.78	66.67	79.80	55.56	55.00	56.25
	2	76.07	44.44	81.82	58.33	60.00	56.25
	3	68.38	27.78	75.76	61.11	65.00	56.25
	4	55.56	61.11	54.55	55.56	60.00	50.00
	5	58.12	66.67	56.57	55.56	60.00	50.00
	6	63.25	66.67	62.63	61.11	70.00	50.00
	7	66.67	66.67	66.67	61.11	70.00	50.00
	8	76.92	66.67	78.79	55.56	60.00	50.00
	9	82.05	72.22	83.84	55.56	60.00	50.00
	10	82.91	72.22	84.85	55.56	60.00	50.00
	11	85.47	77.78	86.87	55.56	60.00	50.00
	12	86.32	83.33	86.87	55.56	60.00	50.00
	13	85.47	83.33	85.86	52.78	60.00	43.75
	14	85.47	83.33	85.86	55.56	65.00	43.75
	15	86.32	83.33	86.87	52.78	60.00	43.75
	16	86.32	83.33	86.87	55.56	65.00	43.75
	17	86.32	83.33	86.87	55.56	65.00	43.75
	18	84.62	83.33	84.85	58.33	70.00	43.75
	19	83.76	83.33	83.84	55.56	65.00	43.75
	20	83.76	83.33	83.84	55.56	65.00	43.75
MIE	1	64.10	88.89	59.60	63.89	65.00	62.50
	2	91.45	94.44	90.91	66.67	65.00	68.75
	3	94.87	100.00	93.94	66.67	70.00	62.50
	4	94.87	100.00	93.94	66.67	70.00	62.50
	5	93.16	100.00	91.92	66.67	70.00	62.50
	6	93.16	100.00	91.92	63.89	70.00	56.25
	7	93.16	100.00	91.92	66.67	70.00	62.50
	8	91.45	100.00	89.90	63.89	70.00	56.25
	9	88.89	100.00	86.87	61.11	70.00	50.00
	10	88.89	100.00	86.87	63.89	70.00	56.25
	11	88.89	100.00	86.87	61.11	75.00	43.75
	12	88.89	100.00	86.87	63.89	70.00	56.25
	13	88.89	100.00	86.87	63.89	70.00	56.25
	14	88.89	100.00	86.87	61.11	70.00	50.00
	15	89.74	100.00	87.88	66.67	70.00	62.50
	16	89.74	100.00	87.88	69.44	75.00	62.50
	17	88.89	100.00	86.87	63.89	75.00	50.00
	18	89.74	100.00	87.88	72.22	70.00	75.00
	19	89.74	100.00	87.88	75.00	75.00	75.00
	20	89.74	100.00	87.88	66.67	70.00	62.50

values of the time series derived from healthy or young subjects were always higher than those from patients or elderly individuals at any scale (Figs. 5–7). Thus, MIE coincides with the complexity-loss theory of ageing and disease over all scales. The consistent MIE results are attributed to the merits of IncrEn. The difference operation in IncrEn for constructing the increment series makes it sensitive to fluctuations in time series. Moreover, MIE naturally characterises the vector pattern with

m points by quantifying the direction and magnitude between adjacent elements. Then, all the patterns are compared to determine the total count for each unique pattern. For the SampEn method, the maximum distance between the corresponding points of two m-dimensional vectors is the only principle for assessing whether they are the same pattern, which is not as comprehensive and natural as IncrEn for complexity analysis of time series.

Furthermore, the time consumption of MSE is the highest, followed by RCMDE and MIE. It is known to all that SampEn requires two nested loops to complete the calculation of the distance between each template vector, thus the time complexity for MSE is $\sum_{\tau=1}^{s} O\left(\frac{N}{\tau}\right)^2$ for the scales ranging from 1 to s, where O is the 'big-O' notation, a commonly used metric for algorithm time complexity, and it assumes the upper bound of the number of steps required for an algorithm to complete. In contrast, there is only one loop in the MIE and RCMDE [26]. However, in order to improve the stability, RCMDE adopted the refined composite idea; therefore, at the τ scale, τ coarse-grained sequences need to be calculated [26]. Therefore, the time complexity for the RCMDE is $\sum_{\tau=1}^{s} \tau O\left(\frac{N}{\tau}\right)$, whereas the time complexity of the MIE is $\sum_{\tau=1}^{s} O\left(\frac{N}{\tau}\right)$. Therefore, the experimental results agree with these facts.

Unlike MSE, MIE has lower variations, and it is always well defined across scales for short time series (data length $= 1,000$), because the data length of the coarse-grained series is less than 100. IncrEn can be used to analyse signals containing at least 100 points [38]. However, SampEn is very sensitive to the parameters for data length $\leqslant 200$ [25]. In addition, MIE shows a certain degree of robustness with dimensions $m = 2$ and $m = 3$, and a resolution of $2 \leqslant R \leqslant 4$, which also inherits the benefits of IncrEn [38]. The stability of MIE is comparable to that of RCMDE, and MSE is the worst among all the indices. The refined composite idea of RCMDE improves the stability, but this leads to a decrease in the efficiency of the method (Table 3).

6. Conclusions

In this research, we further advance the research into MSE and propose MIE after considering existing work along this line, especially multiscale analysis and IncrEn. From the experiments on simulated time series and real-world time series, the proposed novel entropy metric exhibits prominent improvements, and the features of our proposed MIE are summarised as follows:

(1) MIE is more consistent with the complexity-loss theory of disease and ageing for various types of physiological signals at different scales than MSE and RCMDE. For unknown physiological signals, MIE does not need to know the signal itself, does not depend on the scale selection, and can provide the trend of the complexity of the time series changing with scale. Thus, MIE is more suitable for the complexity analysis of unknown physiological signals.
(2) MIE demonstrates better discrimination ability than MSE and RCMDE among physiological conditions known to alter the complexity of the physiological time series.
(3) The robustness of the MIE to the parameters is also better than that of MSE and RCMDE.
(4) In terms of time consumption, MIE was the most efficient, followed by RCMDE and MSE.

A prominent merit of MIE arises from the fact that IncrEn is based on the natural fluctuations of the time series. MIE considers the structures of signals comprehensively and naturally by depicting the directions and amplitudes of fluctuations of signals in an integrated manner, which makes it more accurate for characterising the complexity of physiological signals.

In future research, we will consider extending the MIE to multivariate scenarios, which is suitable for analysing time series collected by multi-channel sensors. Furthermore, we consider extending the MIE to two-dimensional image complexity analysis. Finally, the analysis and applications of MIE in other time-varying volatility time series are worth further investigation as well.

CRediT authorship contribution statement

Xue Wang: Methodology, Software, Validation, Investigation, Formal analysis, Visualization, Writing – original draft. **Xiaofeng Liu:** Conceptualization, Methodology, Supervision, Project administration, Funding acquisition. **Wei Pang:** Writing – review & editing. **Aimin Jiang:** Writing – review & editing.

Declaration of Competing Interest

The authors declare that they have no known competing financial interests or personal relationships that could have appeared to influence the work reported in this paper.

Acknowledgments

This study was supported partially by the National Key Research and Development Program 2018AAA0100800; Key Research and Development Program of Jiangsu under grants BK20192004, BE2018004-04; and International and Exchanges of Changzhou under grant CZ20200035.

References

[1] A.L. Goldberger, C.K. Peng, L.A. Lipsitz, What is physiologic complexity and how does it change with aging and disease?, Neurobiol Aging 23 (1) (2002) 23–26.
[2] T. Nakamura, K. Kiyono, H. Wendt, P. Abry, Y. Yamamoto, Multiscale analysis of intensive longitudinal biomedical signals and its clinical applications, Proc. IEEE 104 (2) (2016) 242–261.
[3] S. Hong, H. Kwon, S.H. Choi, K.S. Park, Intelligent system for drowsiness recognition based on ear canal electroencephalography with photoplethysmography and electrocardiography, Inf. Sci. (2018), S0020025518302561.
[4] M. Hammad, R. Kandala, A. Abdelatey, M. Abdar, P. Pawiak, Automated detection of shockable ecg signals: A review, Inf. Sci. 571 (2021) 580–604.
[5] B.K. Pradhan, K. Pal, Statistical and entropy-based features can efficiently detect the short-term effect of caffeinated coffee on the cardiac physiology, Med. Hypotheses 145 (2020) 110323.
[6] R.D. Dias, M.A. Zenati, R. Stevens, J.M. Gabany, S.J. Yule, Physiological synchronization and entropy as measures of team cognitive load, J. Biomed. Inform. 96 (2019) 103250.
[7] P.T. Krishnan, A.N. Joseph Raj, P. Balasubramanian, Y. Chen, Schizophrenia detection using multivariateempirical mode decomposition and entropy measures from multichannel EEG signal, Biocybern. Biomed. Eng. 40 (3) (2020) 1124–1139.
[8] J. Zhang, Z. Wei, J. Zou, H. Fu, Automatic epileptic EEG classification based on differential entropy and attention model, Eng. Appl. Artif. Intell. 96 (2020) 103975.
[9] D. Cuesta-Frau, P. Miró-Martínez, S. Oltra-Crespo, J. Jordán-Núñez, B. Vargas, L. Vigil, Classification of glucose records from patients at diabetes risk using a combined permutation entropy algorithm, Comput. Methods Programs Biomed. 165 (2018) 197–204.
[10] L. Zhang, X.-H. Wang, L. Li, Diagnosing autism spectrum disorder using brain entropy: A fast entropy method, Comput. Methods Programs Biomed. 105240 (2019).
[11] S.M. Pincus, Approximate entropy as a measure of system complexity, Proc. Natl. Acad. Sci. U.S.A. 88 (6) (1991) 2297–2301.
[12] J.S. Richman, J.R. Moorman, Physiological time-series analysis using approximate entropy and sample entropy, Ajp Heart Circulatory Physiol. 278 (6) (2000) H2039–H2049.
[13] M. Costa, A.L. Goldberger, C.K. Peng, Multiscale entropy analysis of biological signals, Phys. Rev. E 71 (2 Pt 1) (2005) 021906.
[14] M. Costa, A.L. Goldberger, C.-K. Peng, Multiscale entropy analysis of complex physiologic time series, Phys. Rev. Lett. 89 (6) (2002) 068102.
[15] M.D. Costa, A.L. Goldberger, C. Peng, Costa, goldberger, and peng reply, Phys. Rev. Lett. 92 (8) (2003) 89804.
[16] J. Escudero, D. Abásolo, R. Hornero, P. Espino, M. López, Analysis of electroencephalograms in alzheimer's disease patients with multiscale entropy, Physiol. Meas. 27 (11) (2006) 1091.
[17] J. Park, S.Y. Kim, C. Kim, A. Cichocki, K. Kim, Multiscale entropy analysis of EEG from patients under different pathological conditions, Fractals 15 (04) (2007) 399–404.
[18] T. Takahashi, R.Y. Cho, T. Murata, T. Mizuno, M. Kikuchi, K. Mizukami, H. Kosaka, K. Takahashi, Y. Wada, Age-related variation in EEG complexity to photic stimulation: A multiscale entropy analysis, Clin. Neurophysiol. 120 (3) (2009) 476–483.
[19] R. Al-Jawahiri, M. Jones, E. Milne, Spontaneous neural activity relates to psychiatric traits in 16p11.2 cnv carriers: An analysis of EEG spectral power and multiscale entropy, J. Psychiatric Res..
[20] H. Wu, P. Hsu, C. Lin, H. Wang, C. Sun, A. Liu, M. Lo, C. Tang, Multiscale entropy analysis of pulse wave velocity for assessing atherosclerosis in the aged and diabetic, IEEE Trans. Biomed. Eng. 58 (10) (2011) 2978–2981.
[21] S.-D. Wu, C.-W. Wu, S.-G. Lin, C.-C. Wang, K.-Y. Lee, Time series analysis using composite multiscale entropy, Entropy 15 (3) (2013) 1069–1084.
[22] S.-D. Wu, C.-W. Wu, S.-G. Lin, K.-Y. Lee, C.-K. Peng, Analysis of complex time series using refined composite multiscale entropy, Phys. Lett. A 378 (20) (2014) 1369–1374.
[23] S. Wang, H. Tang, B. Wang, J. Mo, Analysis of fatigue in the biceps brachii by using rapid refined composite multiscale sample entropy, Biomed. Signal Process. Control 67 (4) (2021) 102510.
[24] A. Humeauheurtier, The multiscale entropy algorithm and its variants: A review, Entropy 17 (5) (2015) 3110–3123.
[25] J.M. Yentes, N. Hunt, K.K. Schmid, J.P. Kaipust, D. Mcgrath, N. Stergiou, The appropriate use of approximate entropy and sample entropy with short data sets, Ann. Biomed. Eng. 41 (2) (2013) 349–365.
[26] H. Azami, M. Rostaghi, D. Abasolo, J. Escudero, Refined composite multiscale dispersion entropy and its application to biomedical signals, IEEE Trans. Biomed. Eng. 99 (2017) 1–1..
[27] D. Li, X. Li, Z. Liang, L.J. Voss, J.W. Sleigh, Multiscale permutation entropy analysis of EEG recordings during sevoflurane anesthesia, J. Neural Eng. 7(4) (2010) 046010–14..
[28] C. Bandt, B. Pompe, Permutation entropy: a natural complexity measure for time series, Phys. Rev. Lett. 88 (17) (2002) 174102.
[29] S.D. Wu, C.W. Wu, A. Humeau-Heurtier, Refined scale-dependent permutation entropy to analyze systems complexity, Physica A 450 (2016) 454–461.
[30] S. A, B. Mc, A. Dm, Automated detection of epileptic seizures using multiscale and refined composite multiscale dispersion entropy, Chaos Solitons Fractals 146 (2021) 110939..
[31] X. Liu, A. Jiang, N. Xu, J. Xue, Increment entropy as a measure of complexity for time series, Entropy 18 (1) (2016) 22.
[32] M. Costa, C.K. Peng, A.L. Goldberger, J.M. Hausdorff, Multiscale entropy analysis of human gait dynamics, Physica A 330 (1) (2003) 53–60.
[33] M. Rostaghi, H. Azami, Dispersion entropy: A measure for time-series analysis, IEEE Signal Process. Lett. 23 (5) (2016) 610–614.
[34] R.G. Andrzejak, K. Lehnertz, F. Mormann, C. Rieke, P. David, C.E. Elger, Indications of nonlinear deterministic and finite-dimensional structures in time series of brain electrical activity: Dependence on recording region and brain state, Phys. Rev. E 64 (6 Pt 1) (2001) 116–126.
[35] A.L. Goldberger, L.A. Amaral, L. Glass, J.M. Hausdorff, P.C. Ivanov, R.G. Mark, J.E. Mietus, G.B. Moody, C.K. Peng, H.E. Stanley, Physiobank, physiotoolkit, and physionet: components of a new research resource for complex physiologic signals, Circulation 101 (23) (2000) E215.
[36] A.S. Bhogal, A.R. Mani, Pattern analysis of oxygen saturation variability in healthy individuals: Entropy of pulse oximetry signals carries information about mean oxygen saturation, Front. Physiol. 8 (2017) 555.
[37] A. Humeauheurtier, C. Wu, S. Wu, Refined composite multiscale permutation entropy to overcome multiscale permutation entropy length dependence, IEEE Signal Process. Lett. 22 (12) (2015) 2364–2367.
[38] X. Liu, X. Wang, X. Zhou, A. Jiang, Appropriate use of the increment entropy for electrophysiological time series, Comput. Biol. Med. 95 (2018) 13–23.
[39] A.L. Goldberger, L.A. Amaral, J.M. Hausdorff, P.C. Ivanov, C.-K. Peng, H.E. Stanley, Fractal dynamics in physiology: alterations with disease and aging, Proc. Natl. Acad. Sci. 99 (suppl 1) (2002) 2466–2472.